Journal of Alloys and Compounds 509 (2011) 3937–3942

Contents lists available at ScienceDirect

Journal of Alloys and Compounds

journal homepage: www.elsevier.com/locate/jallcom

Spectroscopic investigation of Dy^{3+}-doped $Li_2Gd_4(MoO_4)_7$ crystal for potential application in solid-state yellow laser

Wang Zhao[a,*], Weiwei Zhou[b], Mingjun Song[c], GuoFu Wang[d], Jianming Du[a], Haijun Yu[a], Jingxia Chen[a]

[a] Department of Physics, Huainan Normal University, Xueyuan Road, Huainan, Anhui 232001, PR China
[b] Department of Chemistry & Chemical Engineering, Huainan Normal University, Huainan, Anhui 232001, PR China
[c] College of Chemical Engineering, Weifang University, Weifang, Shandong 261061, PR China
[d] Key Laboratory of Optoelectronic Materials Chemistry and Physics, Fujian Institute of Research on the Structure of Matter, Chinese Academy of Sciences, Fuzhou, Fujian 350002, PR China

ARTICLE INFO

Article history:
Received 2 September 2010
Received in revised form
22 December 2010
Accepted 25 December 2010
Available online 31 December 2010

PACS:
42.70.Hj
78.20.−e

Keywords:
Optical materials
Crystal growth
Optical properties
Luminescence

ABSTRACT

Dy^{3+}:$Li_2Gd_4(MoO_4)_7$ crystal with dimensions of $\varnothing 20 \times 25\,mm^3$ has been grown by the Czochralski method. The spectroscopic properties of Dy^{3+}:$Li_2Gd_4(MoO_4)_7$ crystal have been investigated. Based on the analysis of polarized absorption spectra in the framework of the Judd–Ofelt theory, the main spectroscopic characteristics, including the phenomenological intensity parameters, spontaneous transition probabilities, fluorescence branching ratios and radiative lifetimes of Dy^{3+} in the crystal, have been determined. The emission cross-sections for the $^4F_{9/2} \rightarrow {}^6H_{13/2}$ transition of special interest for laser application have been calculated using the Füchtbauer–Ladenburg (F–L) equation. The fluorescence and radiative lifetimes of $^4F_{9/2}$ manifold are equal to 126.5 μs and 201.1 μs, respectively, which mean the quantum efficiency is 62.9%. The results propose the possibility of Dy^{3+}:$Li_2Gd_4(MoO_4)_7$ crystal for solid-state yellow laser pumped by commercially available blue laser diodes.

1. Introduction

In recent years, there has been renewed interest in optical materials doped with Dy^{3+} ions due to the perspective of developing new laser media for the near-infrared (NIR) and visible regions, or NIR saturable absorber for Q-switch devices [1–4]. As we all known, there is still a blank region between 550 and 650 nm, which cannot be covered even with the Ti:Al_2O_3 laser and its second harmonic, while the yellow laser emission has potential application in a variety of scientific and technological fields, such as military, telecommunication, and commercial. Not until 2000, Kaminskii et al. demonstrated yellow laser operation of Dy^{3+}-doped tungstates in a novel laser channel: $^4F_{9/2} \rightarrow {}^6H_{13/2}$ (~570 nm), at liquid nitrogen temperature under Xe-flashlamp pumping for the first time [1]. As a consequence, the Dy^{3+}-doped crystal materials have been widely investigated [5–15].

$Li_2Gd_4(MoO_4)_7$ crystal belongs to the tetragonal system with $a = 5.192$ Å, $c = 11.30$ Å [16]. Single crystal of $Li_2Gd_4(MoO_4)_7$ was first mentioned as a new paramagnetic ferroelectric crystal [16,17]. However, it was subsequently stated that $Li_2Gd_4(MoO_4)_7$ was not a new ferroelectric but rather a defect scheelite with the formula $Li_{0.286}Gd_{0.571}\varnothing_{0.143}MO_4$ ($\varnothing$ stands for the vacancies in the cation site) [18]. Subsequently, the growth and certain properties of $Li_2Gd_4(MoO_4)_7$ crystal were investigated in Refs. [19,20]. Recently, it was regarded as a promising laser gain medium [21–23]. When Nd^{3+}:$Li_2Gd_4(MoO_4)_7$ crystal microchip was pumped by a Ti:sapphire laser, the maximum 514 mW quasi-cw laser output around 1060 nm was obtained with the slope efficiency of 32% [22]. The $Li_2Gd_4(MoO_4)_7$ crystals doped with rare-earth ions are characterized with the inhomogeneous broadening of the absorption and emission spectra due to structural disorder, which bring a number of advantages from the point of view of applications as active media in LD-pumped solid-state lasers. To our knowledge, the spectral properties of Dy^{3+}:$Li_2Gd_4(MoO_4)_7$ crystal have not been presented. Herein, this paper reports the growth and spectral characteristics of Dy^{3+}:$Li_2Gd_4(MoO_4)_7$ crystal.

2. Experimental

Since $Li_2Gd_4(MoO_4)_7$ crystal melts congruently [18], the $Li_2Gd_4(MoO_4)_7$ crystal doped with 2 at.% Dy^{3+} was grown by the Czochralski method. The raw materials with the composition $Li_2Gd_{3.92}Dy_{0.08}(MoO_4)_7$ were synthesized by the solid-state

* Corresponding author. Tel.: +86 554 6673717; fax: +86 554 6672521.
E-mail address: zwwwz@live.com (W. Zhao).

0925-8388/$ – see front matter © 2010 Elsevier B.V. All rights reserved.
doi:10.1016/j.jallcom.2010.12.176

Fig. 1. Dy^{3+}:$Li_2Gd_4(MoO_4)_7$ crystal grown by the Czochralski method.

reaction with 1 wt.% excess amount of MoO_3 to compensate for the evaporation of MoO_3 during the solid-state reaction and crystal growth. The crystal growth procedure can be found in our previous work [23]. Finally, the Dy^{3+}:$Li_2Gd_4(MoO_4)_7$ crystal with dimension of $\varnothing 20 \times 25\,mm^3$ was obtained, as shown in Fig. 1.

A sample cut from the medium of the as-grown crystal was applied to measure the Dy^{3+} concentration in the crystal. The Dy^{3+} concentration was determined to be 0.63 wt.%, i.e. $1.28 \times 10^{20}\,cm^{-3}$ by inductively coupled plasma and atomic emission spectrometry (ICP-AES). The segregation coefficient K of Dy^{3+} ion in the crystal can be expressed as:

$$K = \frac{C_{sol}}{C_{liq}} \tag{1}$$

where C_{sol} and C_{liq} are the concentrations of Dy^{3+} ions in the solid and liquid phases, respectively. Thus, the segregation coefficient K of Dy^{3+} in Dy^{3+}:$Li_2Gd_4(MoO_4)_7$ crystal is 0.85.

A sample with dimension of 8 mm × 5 mm × 3.1 mm cut from the as-grown crystal was used for the spectral measurement. The polarized absorption spectra were measured using a Perkin-Elmer UV-VIS-NIR Spectrometer (Lambda-900) in 350–2000 nm wavelength range at ambient temperature. The polarized fluorescence spectra and fluorescence lifetime were recorded using an Edinburgh Analytical Instruments FLS920 Fluorescence Spectroscopy.

3. Results and discussion

3.1. Absorption spectra and J–O analysis

Fig. 2 illustrates polarized absorption spectra of the Dy^{3+}:$Li_2Gd_4(MoO_4)_7$ crystal at the room temperature. All the absorption bands are attributed to the transitions of Dy^{3+} ions from the ground state $^6H_{15/2}$ to the excited state J' manifolds, which are marked in Fig. 2. The peak absorption cross-sections at 809 nm are calculated to be $1.09 \times 10^{-20}\,cm^2$ for π-polarization and $0.65 \times 10^{-20}\,cm^2$ for σ-polarization, respectively, which are slightly larger than those of Dy^{3+}:KPb_2Cl_5 ($0.35–0.73 \times 10^{-20}\,cm^2$) [7] and Dy^{3+}:$NaGd(WO_4)_2$ ($0.91 \times 10^{-20}\,cm^2$ for π-polarization and $0.76 \times 10^{-20}\,cm^2$ for σ-polarization) [13]. The full widths at half maximum (FWHM) of absorption band are 8 nm and 10 nm for π- and σ-polarization, respectively. The wide absorption band indicates that the crystal can accommodate some shift of the laser output wavelength of AlGaAs diode laser ($\lambda \approx 808$ nm) with temperature and keep the output laser power stable. In

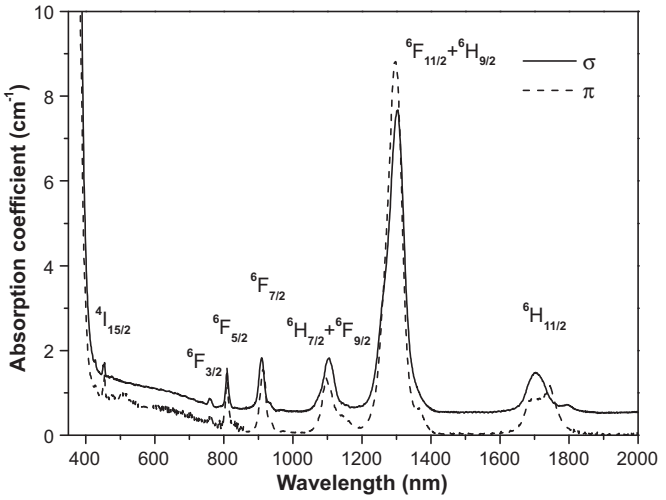

Fig. 2. Polarized absorption spectra of Dy^{3+}:$Li_2Gd_4(MoO_4)_7$ crystal at room temperature. The σ spectrum has been vertically displaced for clarity.

past studies, little attention was paid to the visible emission originating in the $^4F_{9/2}$ manifold due to the fact that the spectral region between the emitting state and the UV absorption edge of matrices is too narrow to ensure efficient population on the higher laser level with classical broad band pumping sources. However, commercialization of blue laser diodes opens new possibilities of optical pumping; therefore, potential laser transitions in the visible are to be reconsidered [6]. The absorption cross-sections of absorption band assigned to $^6H_{15/2} \rightarrow {}^4I_{15/2}$ transition at 450 nm, which is suitable for blue laser diodes pumping, are also estimated to be $0.44 \times 10^{-20}\,cm^2$ for the π-polarization and $0.25 \times 10^{-20}\,cm^2$ for the σ-polarization.

The Judd–Ofelt theory is the most popular method for estimating the spectroscopic parameters of rare-earth ions in crystals and glasses [24,25]. The intensity parameters Ω_t ($t = 2, 4, 6$) can be calculated from the absorption spectra, and then the spontaneous emission probability, fluorescence branching ratios and radiative lifetimes of the excited manifolds can be estimated.

The experimental oscillator strength f_{exp} for the transition from the ground $^6H_{15/2}$ ($J = 15/2$) manifold to the excited J' manifolds can be calculated from the absorption spectra using the formula:

$$f_{exp} = \frac{mc^2}{\pi e^2 \bar{\lambda}_{abs}^{-2} N_0} \int \alpha(\lambda) d\lambda \tag{2}$$

where m and e are the electron mass and charge, respectively; c is the velocity of light; N_0 is the concentration of Dy^{3+} in the crystal, which is 1.28×10^{20} ions/cm^3; $\bar{\lambda}_{abs}$ is the mean wavelength of the absorption band and $\int \alpha(\lambda) d\lambda$ is the integrated absorption coefficient.

For the Dy^{3+} ions, magnetic-dipole transitions also exist besides electric-dipole transitions. For example, the absorption transition $^6H_{15/2} \rightarrow {}^4I_{15/2}$ contains significant contribution of magnetic-dipole component. The magnetic-dipole contribution to the transition strength for $^6H_{15/2} \rightarrow {}^4I_{15/2}$ transition was calculated and subtracted from the measured transition strength to give the pure electric-dipole transition strength according to the following formula:

$$f_{ed}(J \rightarrow J') = f_{exp} - f_{md} \tag{3}$$

$$f_{md}(J \rightarrow J') = \frac{nh}{6mc\bar{\lambda}_{abs}(2J+1)} \times \left| \left\langle 4f^n \alpha\,[LS]J \left\| L + 2S \right\| 4f^n \alpha\,\left[L'S'\right]J' \right\rangle \right|^2 \tag{4}$$

Table 1
Measured and calculated oscillator strengths of Dy^{3+}:$Li_2Gd_4(MoO_4)_7$ crystal at room temperature (md: magnetic-dipole contribution).

Transitions	$f(10^{-6})$, π-polarization					$f(10^{-6})$, σ-polarization				
$^6H_{15/2}\rightarrow$	f_{exp}	f_{cal} (set 1)	Δf(set 1)	f_{cal} (set 2)	Δf(set 2)	f_{exp}	f_{cal} (set 1)	Δf(set 1)	f_{cal} (set 2)	Δf(set 2)
$^4I_{15/2}$	1.33	1.14^{ed} 0.12^{md}	0.07	1.11^{ed} 0.12^{md}	0.10	0.86	0.87^{ed} 0.13^{md}	−0.14	0.85^{ed} 0.13^{md}	−0.12
$^6F_{3/2}$	0.35	0.30	0.05	0.34	0.01	0.27	0.21	0.06	0.24	0.03
$^6F_{5/2}$	1.81	1.58	0.23	1.78	0.03	1.30	1.09	0.21	1.28	0.02
$^6F_{7/2}$	3.62	3.39	0.23	3.64	−0.02	2.81	2.58	0.23	2.83	−0.02
$^6F_{9/2}+{}^6H_{7/2}$	4.22	4.28	−0.06	4.21	0.01	3.73	3.79	−0.06	3.73	0
$^6H_{9/2}+{}^6F_{11/2}$	26.72	26.70	0.02	–	–	23.06	23.04	0.02	–	–
$^6H_{11/2}$	2.98	3.13	−0.15	2.98	0	2.34	2.48	−0.14	2.33	0.01
rms Δf		2.10×10^{-7}		1.32×10^{-7}			1.86×10^{-7}		0.27×10^{-7}	

Set 1 and set 2 are related to the data with and without a hypersensitive transition, respectively.

where the f_{ed} and f_{md} are the oscillator strengths of electric-dipole transitions and magnetic-dipole transitions, respectively. h is the Planck constant, and f_{md} are calculated according to Refs. [26,27]. n is the refractive index. The values of the refractive index reported in Ref. [19] were used to fit the following Sellmeier equations:

$$n_o^2 = 1 + \frac{2.96911\lambda^2}{\lambda^2 - 0.02813} \quad (5)$$

$$n_e^2 = 1 + \frac{2.93595\lambda^2}{\lambda^2 - 0.02849} \quad (6)$$

where λ represents the wavelength (unit: μm). In the subsequent calculation, the values of ordinary and extraordinary refractive indices of the $Li_2Gd_4(MoO_4)_7$ crystal are used for the σ- and π-polarized spectra, respectively.

In the framework of the Judd–Ofelt theory, the oscillator strengths for an electric-dipole transition between states $4f^n[L,S]J$ and $4f^n[L',S']J'$ are expressed as follows:

$$f_{ed}(J\rightarrow J') = \frac{8\pi^2 mc}{3h(2J+1)\bar{\lambda}_{abs}}\frac{(n^2+2)^2}{9n} \times \sum_{t=2,4,6}\Omega_t\left|\left\langle 4f^n[L,S]J\left\|U^{(t)}\right\|4f^n\left[L',S'\right]J'\right\rangle\right|^2 \quad (7)$$

where $U^{(t)}$ (t = 2, 4, 6) is the reduced matrix elements of unit tensor operators, which are almost insensitive to the ion environment. They have been taken from Ref. [28] for the calculations. After obtained the f_{exp} and f_{md} from Eqs. (2) and (4), the f_{ed} can be obtained from Eq. (3). Thus, the intensity parameters Ω_t (t = 2, 4, 6) can be derived from the electric dipole contributions of the experimental oscillator strengths by a least-square fitting of Eqs. (3) and (7). Taking advantage of Eq. (7) and the obtained Ω_t value, the calculated oscillator strength f_{cal} can be determined. Then, the experimental and calculated oscillator strengths are listed in Table 1.

The intensity parameters Ω_t (t = 2, 4, 6) obtained are $\Omega_2 = 23.80\times10^{-20}\,cm^2$, $\Omega_4 = 2.51\times10^{-20}\,cm^2$, $\Omega_6 = 2.70\times10^{-20}\,cm^2$ for π-polarization and $\Omega_2 = 19.99\times10^{-20}\,cm^2$, $\Omega_4 = 2.90\times10^{-20}\,cm^2$, $\Omega_6 = 1.84\times10^{-20}\,cm^2$ for σ-polarization, respectively. Compared with Dy^{3+}-doped other crystals and glasses [6], the values of the Ω_2 parameter for Dy^{3+}:$Li_2Gd_4(MoO_4)_7$ crystal are high. This phenomenon is also mentioned in Ref. [11]. This is because we does not take into consideration the peculiarity of the so-called hypersensitive transitions that obey the following selection rules: $|\Delta S| = 0$, $|\Delta L| \le 2$ and $|\Delta J| \le 2$. These transitions are very sensitive to the environment and are usually intense than the others. Considering the reduced matrix elements involved in the J–O calculations [28], it can be concluded that the value of the Ω_2 parameter exclusively depends on the intensity of the hypersensitive $^6H_{15/2}\rightarrow F_{11/2}$ absorption band and that also the Ω_4 value is strongly related to this transition. It seems that J–O theory does not work well when hypersensitive transitions dominate the spectrum. Therefore, we also carried out the calculation for absorption data without a hypersensitive transition.

The quality of our fitting was measured by means of the root-mean-square deviation between the experimental and calculated oscillator strengths, which is defined as:

$$rms\,\Delta f = \sqrt{\frac{\sum_{i=1}^{N}(f_{exp}-f_{cal})^2}{N-3}} \quad (8)$$

where N is the number of transitions involved in the calculations above.

As a result, the better fitting between experimental and calculated values of oscillator strengths was observed when a hypersensitive transition was excluded from the calculations. The root-mean-square deviation decreases dramatically as shown in Table 1. The intensity parameters Ω_t (t = 2, 4, 6) were found to be $\Omega_2 = 19.51\times10^{-20}\,cm^2$, $\Omega_4 = 1.96\times10^{-20}\,cm^2$, $\Omega_6 = 3.03\times10^{-20}\,cm^2$ for π-polarization and $\Omega_2 = 15.90\times10^{-20}\,cm^2$, $\Omega_4 = 2.38\times10^{-20}\,cm^2$, $\Omega_6 = 2.16\times10^{-20}\,cm^2$ for σ-polarization, when the $^6H_{15/2}\rightarrow{}^6F_{11/2}$ transition was not included. Therefore, the Ω_t obtained from absorption data without a hypersensitive transition was used for further calculations. In Table 2, the Judd–Ofelt parameters that result from the above mentioned analysis are compared with the values obtained for several laser crystals containing Dy^{3+}. The spectroscopic quality factor, $X = \Omega_4/\Omega_6$, first introduced by Kaminskii [29], is also an important laser characteristic in predicting the stimulated emission in laser active medium. The spectroscopic quality factors for Dy^{3+} in $Li_2Gd_4(MoO_4)_7$ are determined to be 0.62 for the π-polarization and 1.10 for the σ-polarization, which fall within the range of 0.37–2.13 for Dy^{3+} doped in different hosts listed in Table 2.

The obtained Judd–Ofelt parameters were used to calculate the total spontaneous emission probabilities A_{total}. The spontaneous emission probability of the electric- and magnetic-dipole transitions between the excited state J' and terminating state J'' of the emission transitions $J'\rightarrow J''$ are given by the following expression:

$$A_{total} = \sum_{J'}\left(A^{ed}_{J'J''} + A^{md}_{J'J''}\right) \quad (9)$$

$$A^{ed(md)}(J'\rightarrow J'') = \frac{8\pi^2 e^2 n^2}{mc\bar{\lambda}^2_{em}} f^{ed(md)}(J'\rightarrow J'') \quad (10)$$

where $\bar{\lambda}_{em}$ is the mean wavelength of emission bands and the values of the reduced matrix elements of unit tensor operators have been given in Ref. [27].

The fluorescence branching ratio of each of the transitions and the radiative lifetime of each of the excited levels can be deter-

Table 2
The J–O intensity parameters of Dy^{3+}-doped crystals.

Crystals	Ω_2 (10^{-20} cm^2)	Ω_4 (10^{-20} cm^2)	Ω_6 (10^{-20} cm^2)	Ω_4/Ω_6	Ref.
Dy^{3+}:BaY_2F_8	1.52	2.33	3.67	0.63	[8]
Dy^{3+}:$Y_3Sc_2Ga_3O_{12}$	0.13	0.73	1.06	0.69	[9]
Dy^{3+}:YVO_4	6.59	3.71	1.74	2.13	[10]
Dy^{3+}:Lu_2SiO_4	4.31	1.28	3.49	0.37	[11]
Dy^{3+}:$YAl(BO_3)_4$	9.49	2.77	2.10	1.33	[9]
Dy^{3+}:$KGd(WO_4)_2$	15.35	3.05	2.01	1.52	[6]
Dy^{3+}:$NaLa(WO_4)_2$	14.43	2.60	1.68	1.55	[12]
Dy^{3+}:$NaY(MoO_4)_2$	15.01	1.98	1.05	1.89	[15]
Dy^{3+}:$CaMoO_4$	26.60	2.89	1.79	1.61	[14]
Dy^{3+}:$Li_2Gd_4(MoO_4)_7$	19.51^{π}	1.96^{π}	3.03^{π}	0.65^{π}	This work
	15.90^{σ}	2.38	2.16^{σ}	1.10^{σ}	

mined from the spontaneous emission probability according to the expressions:

$$\beta_{J'J''} = \frac{A^{ed}_{J'J''} + A^{md}_{J'J''}}{A_{total}} \tag{11}$$

$$\tau_r = \frac{1}{A_{total}} \tag{12}$$

Then the calculated electric and magnetic dipole spontaneous emission probabilities, radiative lifetimes, and branching ratios for the main emission transitions of Dy^{3+} in $Li_2Gd_4(MoO_4)_7$ crystal, are summarized in Table 3. In the case of $^4F_{9/2}$ manifold, the highest calculated value of the fluorescence branching ratio corresponds to $^4F_{9/2} \rightarrow {}^6H_{13/2}$ transition at 575 nm, which means yellow emission should dominate the emission spectrum. It suggests that this transition could give rise to lasing action.

3.2. Fluorescence spectra and stimulated emission cross-sections

Fig. 3 displays the fluorescence spectra of Dy^{3+}:$Li_2Gd_4(MoO_4)_7$ crystal at room temperature, which was excited by the steady state xenon lamp (Xe900, Edinburgh) at 455 nm. Four fluorescence bands centered around 480 nm, 575 nm, 660 nm and 750 nm are assigned to the $^4F_{9/2} \rightarrow {}^6H_{15/2}$, $^4F_{9/2} \rightarrow {}^6H_{13/2}$, $^4F_{9/2} \rightarrow {}^6H_{11/2}$ and $^4F_{9/2} \rightarrow {}^6H_{9/2} + {}^6F_{11/2}$ transitions, respectively. To assess the spectral distribution originating in the $^4F_{9/2}$ manifold, the experiment fluorescence branching ratios β_{exp} were evaluated by integration

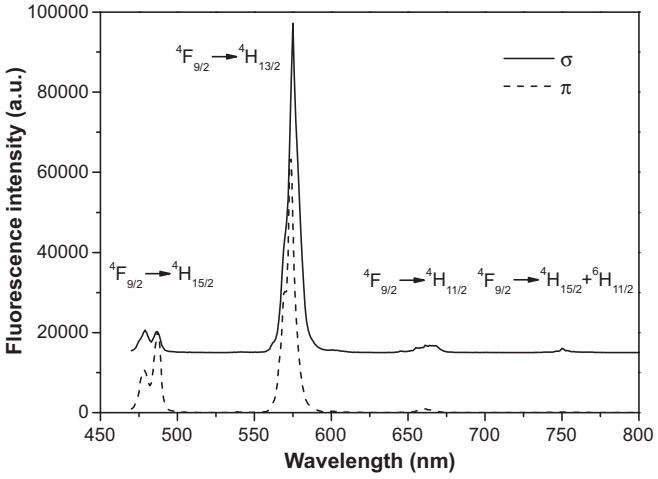

Fig. 3. Polarized fluorescence spectra of Dy^{3+}:$Li_2Gd_4(MoO_4)_7$ crystal at room temperature. The σ spectrum has been vertically displaced for clarity.

of the fluorescence spectrum using the following formula:

$$\beta = \frac{\int_a^b I(\lambda)d\lambda}{\int_0^\infty I(\lambda)d\lambda} \tag{13}$$

It should be noticed that only four luminescence bands have been recorded in this paper. Accordingly, we neglected weak transitions in the infrared region and assumed the total emission intensity integration in four measured bands as 100% [6]. Table 4 exhibits experiment branching ratio β_{exp} and calculated branching ratio β_{cal} determined by the J–O analysis for the $^4F_{9/2} \rightarrow {}^6H_{13/2}$ emission in several hosts doped with Dy^{3+}. It can be observed the values of β_{exp} for Dy^{3+}:$Li_2Gd_4(MoO_4)_7$ crystal are higher than other crystals and glasses listed in Table 4. In general, the luminescence branching ratio β is a critical parameter to the laser designer, because it characterizes the possibility of attaining stimulated emission for any specific transition. The experiment branching ratios β_{exp} for the $^4F_{9/2} \rightarrow {}^6H_{13/2}$ transition are found to be 0.711 and 0.875 for π- and σ-polarization, respectively, suggesting that that the yellow emission intensity on the transition ($^4F_{9/2} \rightarrow {}^6H_{13/2}$) at 575 nm is much more intense than that of other transitions, and it is of interest for application. In addition, it can be seen from Table 4 that the difference between β_{exp} and β_{cal} may be obvious for some hosts. For example, β_{exp} = 0. 539, β_{cal} = 0.653 was reported for Dy^{3+}:$LiNbO_3$ crystal [6] and β_{exp} = 0.578, β_{cal} = 0.762 was reported for Dy^{3+}-doped fluorophosphates glass [30]. The similar instance also happed in Dy^{3+}:$Li_2Gd_4(MoO_4)_7$ crystal for σ-polarization, although β_{exp} matches well with β_{cal} for π-polarization. The intrinsic uncertainty of Judd–Ofelt calculation (±30%) is large enough to explain the deviation between β_{exp} and β_{cal} for the $^4F_{9/2} \rightarrow {}^6H_{13/2}$ transition.

The stimulated emission cross sections σ_{em} of $^4F_{9/2} \rightarrow {}^6H_{13/2}$ transition can be determined by the fluorescence spectrum using the Füchtbauer–Ladenburg (F–L) formula [32]:

$$\sigma_{em} = \frac{\lambda^5 \beta}{8\pi n^2 c} \frac{1}{\tau_r} \frac{I(\lambda)}{\int \lambda I(\lambda)d\lambda} \tag{14}$$

where n is the refractive index, c is the speed of light, $I(\lambda)$ is the fluorescence intensity at wavelength λ. Thus, the wavelength dependence of cross-sections σ_{em} for the transition $^4F_{9/2} \rightarrow {}^6H_{13/2}$ is shown in Fig. 4, and the maximal emission cross-sections σ_{em} at 575 nm were determined to be 1.34×10^{-20} cm^2 for π-polarization and 1.45×10^{-20} cm^2 for σ-polarization. These values are higher than those of most of other materials investigated (0.78×10^{-20} cm^2 for Dy^{3+}:YVO_4 [10], 0.74×10^{-20} cm^2 for Dy^{3+}:Lu_2SiO_4 [11], 1.04×10^{-20} cm^2 for Dy^{3+}:$NaLa(WO_4)_2$ [12] and 0.36×10^{-20} cm^2 for Dy^{3+}:fluorogermanate glass[6]), and slightly lower than that of Dy^{3+}:$YAl(BO_3)_4$ (1.90×10^{-20} cm^2 for σ-polarization) [6]. By the way, Dy^{3+}:$YAl(BO_3)_4$ crystal offer the highest value of cross-sections ever reported for the $^4F_{9/2} \rightarrow {}^6H_{13/2}$

Table 3
Calculated spontaneous emission probabilities, radiative branching ratios and radiative lifetime in Dy^{3+}:$Li_2Gd_4(MoO_4)_7$ crystal.

Transition $^4F_{9/2}\rightarrow$	λ_{em} (nm)	π-Polarization			σ-Polarization			τ_{rad} (μs)
		A_{ed} (S^{-1})	A_{md} (S^{-1})	β (%)	A_{ed} (S^{-1})	A_{md} (S^{-1})	β (%)	
$^6F_{5/2}$	1156	48.55		0.86	40.36		0.87	201.05
$^6F_{7/2}$	992	13.22	11.54	0.44	12.36	11.69	0.52	
$^6H_{5/2}$	918	8.31		0.15	8.80		0.19	
$^6H_{7/2}$	836	56.54	6.65	1.12	51.04	6.72	1.24	
$^6F_{9/2}$	831	29.39	11.76	0.73	28.80	11.90	0.88	
$^6F_{11/2}$	748	120.00	108.56	4.07	101.88	109.87	4.55	
$^6H_{9/2}$	747	86.81	6.24	1.66	72.98	6.32	1.71	
$^6H_{11/2}$	661	424.52	28.85	7.97	360.41	24.71	8.28	
$^6H_{13/2}$	574	4042.20		71.88	3345.39		71.96	
$^6H_{15/2}$	487	625.59		11.12	455.68		9.80	

Table 4
Fluorescence branching ratios of the $^4F_{9/2} \rightarrow {}^6H_{13/2}$ emissions in Dy^{3+}-doped hosts.

	$Li_2Gd_4(MoO_4)_7$		$YAl_3(BO_3)_4$	$LiNbO_3$	Fluoro-germinate glass	Fluoro-phosphate glass	Fluoro-zicronate glass
	π	σ					
β_{exp}	71.1	87.5	64.7	53.9	70.1	57.8	48.0
β_{cal}	71.9	72.0	65.9	65.5	66.3	72.6	61.0
Ref.	This work		[6]	[6]	[6]	[30]	[31]

transition in Dy^{3+}-doped matrices, which was regarded as the most promising material for yellow laser operation among the crystals and glasses investigated by Ryba-Romanowski [6]. It is noteworthy that the calculated values depend on incertitude associated with radiative transition rates derived from a fitting procedure in the framework of the Judd–Ofelt theory. Therefore, the calculated emission cross-sections should be treated as estimated values to be verified by laser experiments.

3.3. Fluorescence lifetime and quantum efficiency

Fig. 5 presents the luminescence decay curve in correspondence with the emission line $^4F_{9/2} \rightarrow {}^6H_{13/2}$ at 575 nm at ambient temperature. The linear relationship displays single exponential behavior of the fluorescence decay, and the fluorescence lifetime of $^4F_{9/2} \rightarrow {}^6H_{13/2}$ transition at 575 nm is found to be 126.5 μs with chi-square of 1.51×10^{-4}. Then the fluorescence quantum efficiency

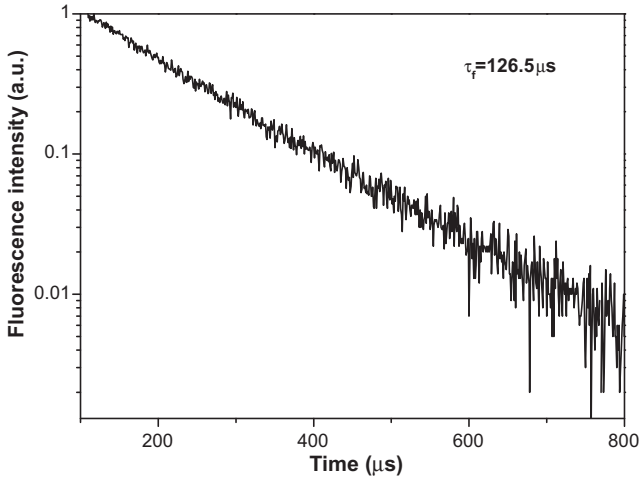

Fig. 4. Fluorescence decay curve of $^4F_{9/2}$ multiplet for Dy^{3+}:$Li_2Gd_4(MoO_4)_7$ crystal at room temperature.

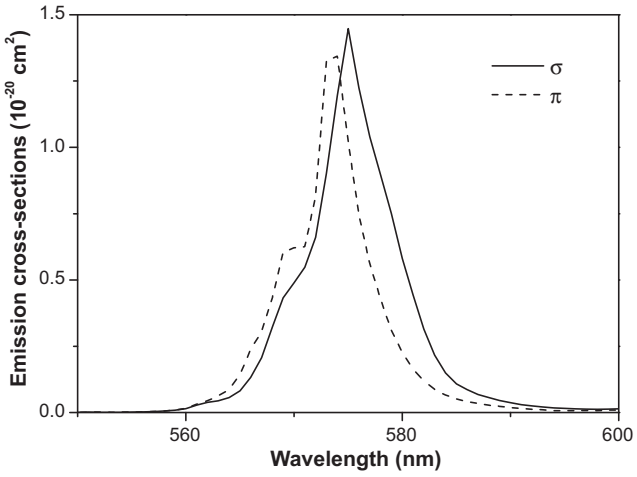

Fig. 5. Emission cross-sections corresponding to the $^4F_{9/2} \rightarrow {}^6H_{13/2}$ transition of Dy^{3+}:$Li_2Gd_4(MoO_4)_7$ crystal.

Table 5
Comparison of the emission spectroscopic parameters of several Dy^{3+}-doped laser crystals.

Crystal	σ_{em} (10^{-20} cm^2)	τ_f (μs)	τ_R (μs)	η (%)	Ref.
Dy^{3+}:$LiNbO_3$	0.32 (σ), 0.03 (π)	298	387	77.0	[6]
Dy^{3+}:YVO_4	–	130	440	29.5	[10]
Dy^{3+}:$YAl_3(BO_3)_4$	1.90 (σ), 0.62 (π)	520	508	>100	[6]
Dy^{3+}:Lu_2SiO_4	0.74	509	635	80.2	[11]
Dy^{3+}:$KGd(WO_4)_2$	190 (150K)	175	160	>100	[5]
Dy^{3+}:$NaLa(WO_4)_2$	1.04 (σ), 1.01(π)	268	292	89.9	[12]
Dy^{3+}:$NaY(MoO_4)_2$	1.21 (σ), 1.04(π)	107	271	39.5	[15]
Dy^{3+}:$CaMoO_4$	–	152	177	85.9	[14]
Dy^{3+}:$Li_2Gd_4(MoO_4)_7$	1.45(σ), 1.34 (π)	126.5	201.1	62.9	This work

η ($\eta = \tau_f/\tau_r$) is derived as 62.9%. This indicates that the multi-phonon relaxation is inefficient, as expected from the fact that the energy gap between the $^4F_{9/2}$ emitting level and the next-lower state (about 7700 cm^{-1}) is large with respect to the maximum phonon energy of the host lattice (~900 cm^{-1} [33]). It is interesting to observe that the fluorescence quantum efficiency η of Dy^{3+}:$Li_2Gd_4(MoO_4)_7$ crystal is lower than that of Dy^{3+}:$YAl_3(BO_3)_4$ crystal [6,34]. Generally, the larger the energy gap and the lower the maximum phonon energy is, the lower nonradiative transition rate is. So the fluorescence quantum efficiency η of molybdates is often higher than those of borates (some specific examples can be referred to in Table 5 of Ref. [35]). Concentration quenching effect may account for this in view of the fact that the fluorescence lifetimes of 0.5% Dy^{3+}:$YAl_3(BO_3)_4$ and 2% Dy^{3+}:$Li_2Gd_4(MoO_4)_7$ were investigated for comparison.

Table 5 shows the emission parameters of the $^4F_{9/2} \rightarrow {}^6H_{13/2}$ transition for the Dy^{3+}:$Li_2Gd_4(MoO_4)_7$ crystal as compared with other Dy^{3+}-doped laser crystals. Based on the above analysis, Dy^{3+}:$Li_2Gd_4(MoO_4)_7$ crystal has high quantum efficient η, large emission cross-sections σ_{em} and fluorescence branching ratio β for the $^4F_{9/2} \rightarrow {}^6H_{13/2}$ transition. These results indicate that it is a potential candidate for laser operation in the yellow region and deserves further investigations in this direction.

4. Conclusions

Dy^{3+}:$Li_2Gd_4(MoO_4)_7$ crystal with dimensions of $\varnothing 20 \times 25\ mm^3$ has been grown by the Czochralski method. Polarized absorption spectra, fluorescence spectra and fluorescence decay curve of Dy^{3+}:$Li_2Gd_4(MoO_4)_7$ have been recorded at room temperature. Based on the Judd–Ofelt theory, the intensity parameters, the spontaneous emission probabilities, fluorescence branching ratios and radiative lifetimes of the excited manifolds were estimated. The peak emission cross-sections σ_{em} for the $^4F_{9/2} \rightarrow {}^6H_{13/2}$ transition were calculated to be $1.34 \times 10^{-20}\ cm^2$ for π-polarization and $1.45 \times 10^{-20}\ cm^2$ for σ-polarization using the Füchtbauer–Ladenburg (F–L) equation. The fluorescence and radiative lifetimes of $^4F_{9/2}$ manifold were 126.5 μs and 201.1 μs, respectively, so the quantum efficiency was 62.9%. The results of these investigations indicate that the Dy^{3+}:$Li_2Gd_4(MoO_4)_7$ crystal may be regarded as a potential solid-state yellow laser material.

Acknowledgements

This project was supported by the Nature Science Foundation of Education Department of Anhui Province (KJ2010B203, KJ2010B205) and Shandong Province Science Foundation for Youths (ZR2010EQ007).

References

[1] L.F. Johnson, H.J. Guggenheim, Appl. Phys. Lett. 23 (1973) 96–98.
[2] P.Y. Tigreat, J.L. Doualan, R. Moncorgé, B. Ferrand, J. Lumin. 94–95 (2001) 107–111.
[3] A.A. Kaminskii, U. Hömmerich, D. Temple, J.T. Seo, K. Ueda, S. Bagayev, A. Pavlyulk, Jpn. J. Appl. Phys. 39 (2000) L208–L211.
[4] M.D. Seltzer, A.O. Wright, C.A. Morrison, D.E. Wortman, J.B. Gruber, E.D. Filer, J. Phys. Chem. Solids 57 (1996) 1175–1182.
[5] A.A. Kaminskii, J.B. Gruber, S.N. Bagaev, K. Ueda, U. Hommerich, J.T. Seo, D. Temple, B. Zandi, A.A. Kornieko, E.B. Dunina, Phys. Rev. B 65 (2002) 125108.
[6] W. Ryba-Romanowski, G. Dominiak-Dzik, P. Solarz, R. Lisiecki, Opt. Mater. 31 (2009) 1547–1554.
[7] M.C. Nostrand, R.H. Page, S.A. Payne, L.I. Isaenko, A.P. Yelisseyev, J. Opt. Soc. Am. B 18 (2001) 264–276.
[8] D. Paris, A. Toncelli, M. Tonelli, E. Cavalli, E. Bovero, A. Belletti, J. Phys.: Condens. Matter 17 (2005) 2783–2790.
[9] D.K. Sardar, W.M. Bradley, R.M. Yow, J.B. Gruber, B. Zandi, J. Lumin. 106 (2004) 195–203.
[10] E. Cavalli, M. Bettinelli, A. Belletti, A. Speghini, J. Alloys Compd. 341 (2002) 107–110.
[11] G. Dominiak-Dzik, W. Ryba-Romanowski, R. Lisiecki, P. Solarz, M. Berkowski, Appl. Phys. B 99 (2010) 285–297.
[12] Y.P. Wei, C.Y. Tu, H.Y. Wang, F.G. Yang, G.H. Jia, Z.Y. You, X.A. Lu, J.F. Li, Z.J. Zhu, Y. Wang, J. Alloys Compd. 438 (2007) 310–316.
[13] H.Y. Wang, J.F. Li, G.H. Jia, Z.Y. You, F.G. Yang, Y.P. Wei, Y. Wang, Z.J. Zhu, X.A. Lu, C.Y. Tu, J. Lumin. 126 (2007) 452–458.
[14] E. Cavalli, E. Bovero, A. Belletti, J. Phys.: Condens. Matter 14 (2002) 5221–5228.
[15] X.A. Lu, Z.Y. You, J.F. Li, Z.J. Zhu, G.H. Jia, B.C. Wu, C.Y. Tu, J. Lumin. 126 (2007) 63–67.
[16] R.K. Pandey, J. Phys. Soc. Jpn. 36 (1974) 177–178.
[17] R.K. Pandey, A.G. Castellanos-Guzmán, Solid State Commun. 25 (1978) 283–288.
[18] L.H. Brixner, J. Phys. Soc. Jpn. 38 (1975) 1218.
[19] O.E. Bochkov, V.M. Gorbenko, Yu.V. Zabara, A.Yu. Kudzin, S.A. Flerova, Sov. Phys. Crystallogr. 22 (1977) 371–372.
[20] E.M. Kostova, M.K. Kostov, Phys. Stat. Sol. (a) 92 (1985) K105–K106.
[21] H.M. Zhu, Y.J. Chen, Y.F. Lin, X.H. Gong, J.S. Liao, X.Y. Chen, Z.D. Luo, Y.D. Huang, J. Phys. D: Appl. Phys. 40 (2007) 6936–6941.
[22] H.M. Zhu, Y.F. Lin, Y.J. Chen, X.H. Gong, Q.G. Tan, Z.D. Luo, Y.D. Huang, J. Appl. Phys. 102 (2007) 063104.
[23] W. Zhao, L.Z. Zhang, G.F. Wang, J. Cryst. Growth 311 (2009) 2336–2340.
[24] B.R. Judd, Phys. Rev. 127 (1962) 750–761.
[25] G.S. Ofelt, J. Chem. Phys. 37 (1962) 511–520.
[26] W.T. Carnall, P.R. Fields, K. Rajnak, J. Chem. Phys. 49 (1968) 4412–4423.
[27] C.K. Jayasankar, E. Rukmini, Phys. B 240 (1997) 273.
[28] W.T. Carnall, P.R. Fields, K. Rajnak, J. Chem. Phys. 49 (1968) 4424.
[29] A.A. Kaminskii, Laser Crystals, Springer, Berlin, 1981.
[30] R. Praavena, R. Vijaya, C.K. Jayasankar, Spectrochim. Acta A 70 (2008) 577–586.
[31] V.M. Orera, P.J. Alonso, R. Cases, R. Alcala, Phys. Chem. Glasses 29 (1988) 59–62.
[32] B.F. Aull, H.P. Jenssen, IEEE J. Quantum Electron. 18 (1982) 925.
[33] T.T. Basiev, A.A. Sobel, Yu.K. Voron, P.G. Zverev, Opt. Mater. 15 (2000) 205–216.
[34] G. Dominiak-Dzik, P. Solarz, W. Ryba-Romanowski, E. Beregi, L. Kovács, J. Alloys Compd. 359 (2003) 51–58.
[35] W. Zhao, L.Z. Zhang, G.J. Wang, M.J. Song, Y.S. Huang, G.F. Wang, Opt. Mater. 31 (2009) 849–853.